DFT STUDIES ON METHYL RED DOPED ZTS CRYSTALS FOR POSSIBLE NONLINEAR OPTICAL APPLICATIONS

G.SURESH[1], P.KUMARESAN[2], S.NIHIYANANTHAM[3], K.SAMBATH KUMAR[4] & P.AMBALAVANAN[5]

[1,2] P.G &Research Department of Physics, Thiru.A.Govindasamy Government Arts College, Tindivanam-604 002, Tamil Nadu, [3,] P.G &Research Department of Physics, Thiru.Vi.Ka. Government Arts College, Thuruvarur, Tamil Nadu, India

[4,5] P.G &Research Department of Physics, Arignar Anna Government Arts College, Villupuram, Tamil Nadu, India

Abstract: ***Zinc Thiourea Sulphate (ZTS), crystal is a magnificent metal natural compound, which consolidates the upsides of both natural and inorganic materials when contrasted and other customary non-linear optical materials and in this way can be utilized as a part of a more extensive scope of uses. Late endeavors at delivering new recurrence transformation materials have concentrated essentially on expanding the extent of the NLO properties that can recurrence twofold low pinnacle control sources, for example, diode lasers. The thermo gravimetric examination (TGA) and differential warm investigation (DTA) were completed utilizing Seiko warm analyzer at warming rate 20°C/min in air to decide the warm dependability of the compound. ZTS crystals were developed by moderate cooling procedure. This empowers the development of mass gems along all the three bearings at an ideal pH. FTIR examines demonstrate that in the spectra of ZTS there is a move in the recurrence band in the low-recurrence district which uncovers that thiourea shapes sulfur-to-zinc securities in the ZTS crystals. The stability and charge delocalization of the molecule were also studied by natural bond orbital (NBO) analysis. The HOMO-LUMO energies describe the charge transfer takes place within the molecule. Molecular electrostatic potential has been analyzed. The developments try in extensive scale with this enhanced pH qualities is required to yield mass crystal appropriate for laser combination tests and SHG device applications.***

Key words: ZTS crystal, FT-IR studies, Thermal studies, HOMO-LUMO studies, SHG measurements

1. INTRODUCTION

Non-linear optical (NLO) materials significantly affect laser innovation, optical correspondence, optical capacity innovation and electro optic adjustment. The hunt down new recurrence change materials over the previous decade has prompted to the disclosure of numerous semiorganic materials [1-3]. These materials groups vast nonlinearity, high resistance laser prompted harm and low precise affectability. The semi natural NLO materials pick up significance over natural and inorganic NLO materials due to their huge polarizability and wide transmission window.

Crystal growth is nothing but the addition of units. The addition can be either by particles or by molecules or atom. Crystal growth is always an art, science, engineering, technology and technique. In a way growing crystals in industries controls our economy. Crystals growing in atmosphere are responsible for rain.

The strong influence of single crystals in the present day technology is evident from the resent advancements of the fields of semiconductors, polarizer's, transducers, infrared detectors, ultrasonic amplifiers, solid state lasers, non-linear optic, piezoelectric, Acosta-optic, photosensitive materials and crystalline thin films for microelectronics and computer industries. Hence to achieve high performance from the device, good quality single crystals are needed. The growth of single crystals and their characterization towards device fabrication has assumed great impetus due to their importance for both academic research and applied research.

To understand the kinetics and mechanisms involved in the process of crystal growth, many theories such as surface energy theory, diffusion theory, surface adsorption theory, etc. have been proposed. The first theory of crystal growth was proposed as early as the late 19th century [4]. The development of the theories of crystal growth has thrown more light on the understanding of crystal growth phenomena. Compared with inorganic NLO materials, organic materials may fulfill many of these requirements, but there are also some drawbacks with organic NLO materials such as environmental stability, poor chemical and mechanical stability, red-shift of the cut-off wavelength, low laser damage thresholds and poor phase matching properties [5-9]. In order to overcome these drawbacks and improve the properties, the growth of semi-organic crystals has nowadays come into prominence [10]. In order to meet this increasing demand of new material with good optical properties, identifying and growth of new optical crystals with good crystalline nature has become an interesting branch in crystal growth[11].Broad examination in this course brought about the disclosure of another stage coordinate inorganic material like ZTS crystals

2. EXPERIMENTAL PROCEDURE

2.1 Crystal Growth

Pure ZTS crystals were grown from aqueous solution by slow evaporation and also by slow cooling method (0.5^0 C/Day). The same method is followed for doped ZTS crystals (0.1 mole % of Methyl Red). The solubility of doped ZTS in the solvent was measured for each dopant, it was found to be 27.5gms/100 ml at 40^oC for Methyl Red. The seed crystals are prepared at low temperature by spontaneous nucleation [12]. The seed crystals (Fig. 1 a,b) with perfect shape and free from macro defects were used for growth experiments. Large single crystals of ZTS and doped ZTS were grown using constant temperature bath (CTB) controlled with an accuracy of 0.01^0C. The mother solution was saturated with the initial pH value, 4.2 for Methyl Red**.** The growth was carried out for more than 21 days by keeping the bath at a temperature of 39^0C.

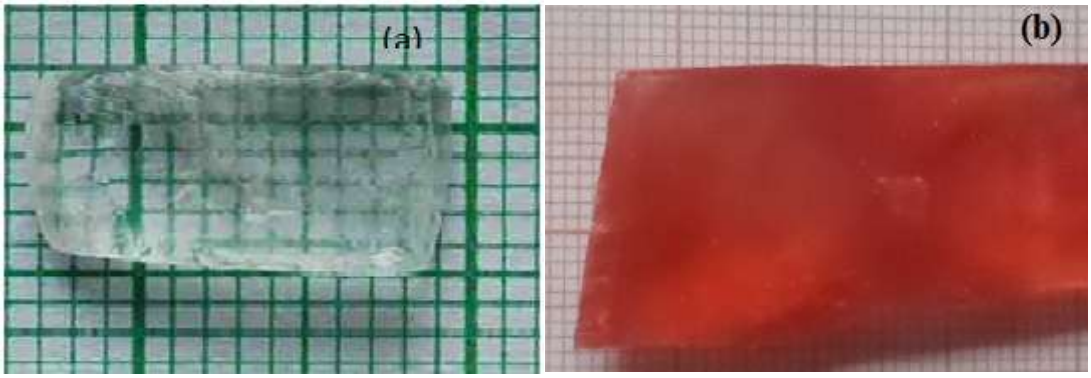

Figure 1. (a) Pure and (b) Methyl Red doped ZTS Crystal

2.2 X-Ray Diffraction Studies

Powder XRD spectra (Fig.2) for the pure and Methyl Red doped ZTS revealed that the structures of the doped crystals are slightly distorted compared to the pure ZTS crystal. This may be attributed to strains on the lattice by the absorption or substitution of dyes. It is observed that the reflection lines of the doped ZTS crystal correlate well with those observed in the individual parent compound with a slight shift in the Bragg angle.

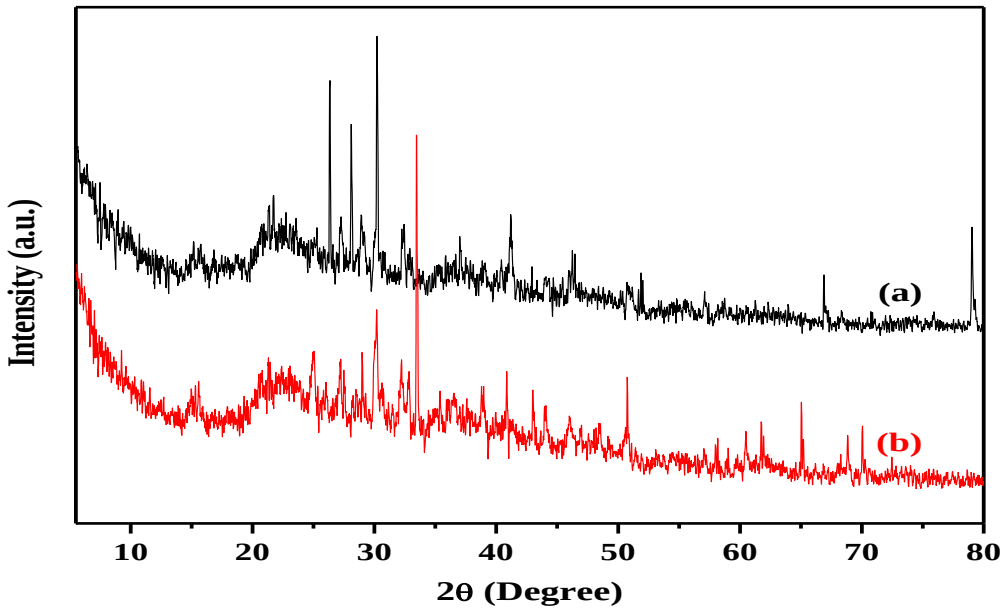

Figure 2 XRD of (a) Pure and (b) Methyl Red doped ZTS crystal

2.3 FT-IR Analysis

The FT-IR range was recorded between 1000 cm^{-1} and 4000 cm^{-1}, utilizing BRUKER IFS 66V FT-IR spectrometer. The FT-IR Spectra of both the unadulterated and doped ZTS precious stones are appeared in Figure 2. The FT-IR spectra of immaculate and doped ZTS show up practically like each other. N-H extending frequencies of amino gathering are found between 3026 cm^{-1} and 2923 cm^{-1} for both unadulterated and doped precious stones. Both the immaculate and doped mixes demonstrate ingestion at 1620 cm^{-1} showing the nearness of essential amino gathering. The trademark ingestion for the - NH gather in the fragrant ring is seen at 2421 cm^{-1} for ZTS. The expansive ingestion around 3000 cm^{-1} demonstrates the co nearness of C=O extending and O-H extending.

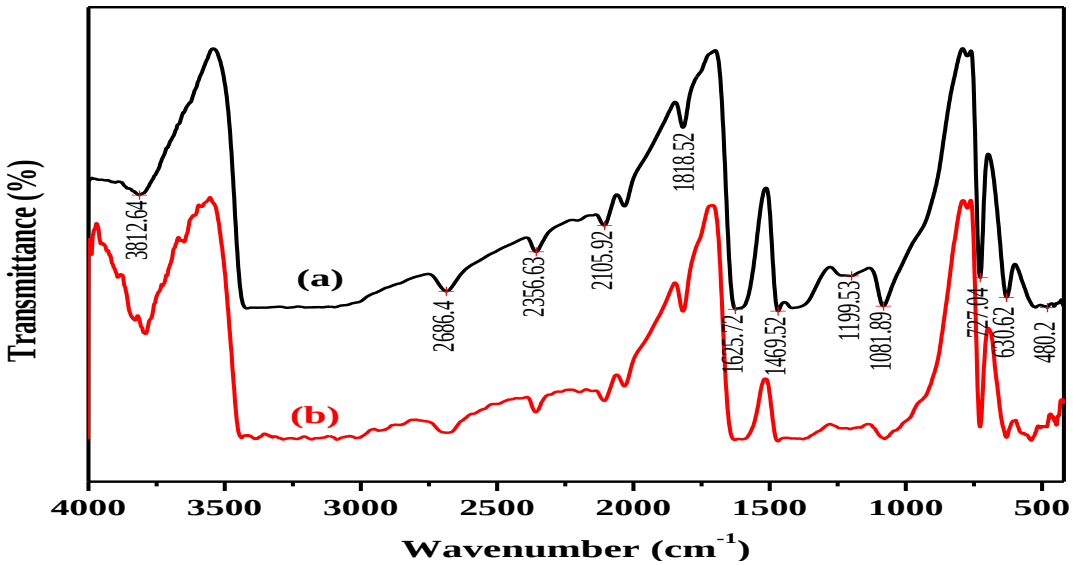

Figure 2. FT-IR spectra of (a) Pure and (b) Methyl Red doped ZTS crystal

The FT-IR spectra of both the pure and doped ZTS affirm the auxiliary viewpoints. Doping of metal particle into the crystal lattices does not demonstrate any centrality change in assimilation design. A portion of the assimilations demonstrate a stamped contrast in rate transmittance. The rate change of transmittance particularly, at 1199 cm^{-1} and 1490 cm^{-1} are important. It is induced that the metal particle, shape powerless linkages in the interstices of the relating crystals.

2.4 MICROHARDNESS STUDIES

Microhardness is one of the essential mechanical properties of the ZTS precious stones. It can be appropriately used to quantify the plastic properties and quality of a material. Microhardness estimations were completed utilizing Leitz Weitzler hardness analyzer fitted with a precious stone indenter (Fig.3). The all around cleaned Methyl Red doped ZTS precious stone was set on the stage of the Vickers small scale hardness analyzer and the heaps of various sizes were connected over an analyzer at a settled interim of time [13]. The space time was kept as 8 sec for every one of the heaps. The microhardness esteem was computed utilizing the connection $H_v = 1.8544 \text{ X } P/d^2$ kg/mm^2, where P is the connected load in kg and d is the corner to corner length of the space impression in mm. Color doping enhances the mechanical quality of ZTS.

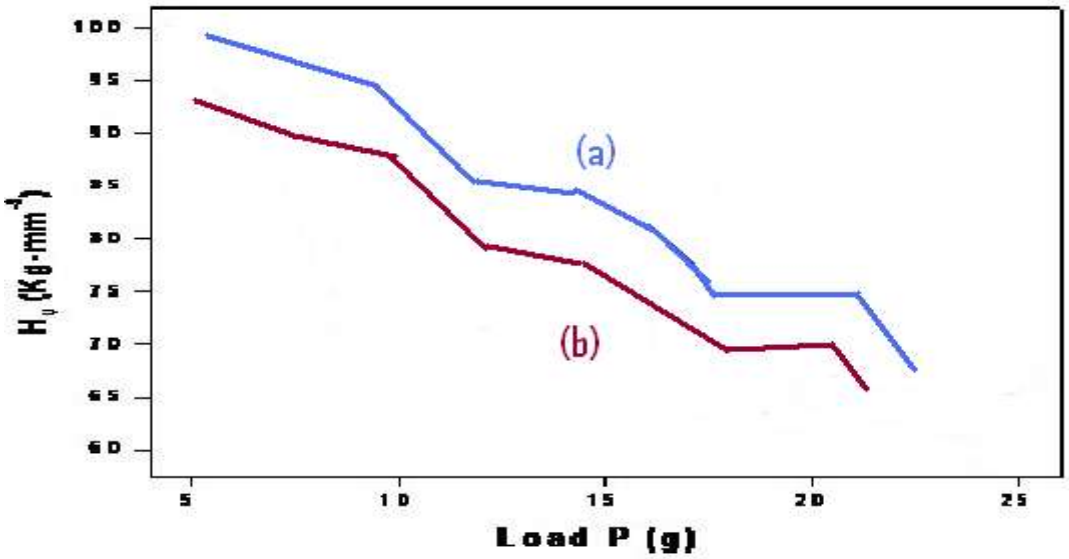

Figure 3. Microhardness studies of (a) Methyl Red doped ZTS and (b) Pure ZTS crystals

2.5 THERMAL STUDIES

Figure 4. shows the Differential Thermal Analysis (DTA) and Thermo-Gravimetric Analysis (TGA) bends for the developed) Methyl Red doped ZTS crystal. The DTA bend infers that the material experiences an irreversible endothermic move at 200°C where the liquefying starts. This pinnacle was endothermic pinnacle, speaks to the temperature at which the dissolving ends which relates to its liquefying point at 210°C. In a perfect world, the liquefying purpose of the follow relates to a vertical line. The sharpness of the endothermic pinnacle indicates great level of crystallinity of the developed ingot [10]. The exothermic crest at 561°C demonstrates a stage change from fluid to vapor state as obvious from the loss of weight of around 87% in TG curve.

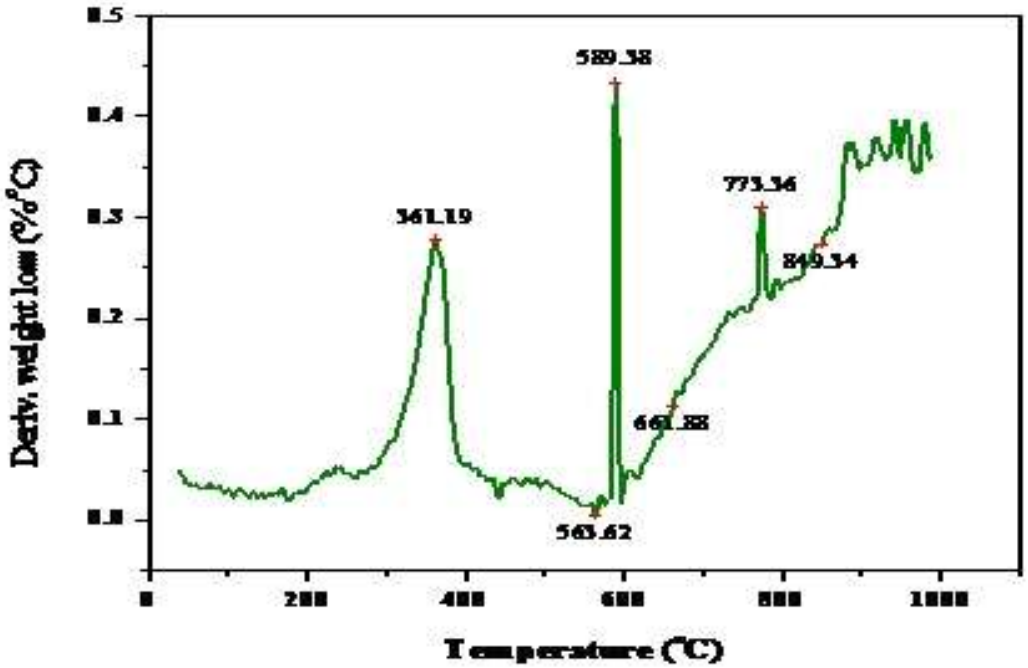

Figure 4. TGA-DTA curves of Methyl Red doped ZTS Crystal

2.6 FRONTIER MOLECULAR ORBITALS

Many organic molecules that contain conjugated π electrons are characterized hyperpolarizabilities and are analyzed by means of vibrational spectroscopy [14]. In most cases, even in the absence of inversion symmetry, the strongest bands in the Raman spectrum are weak in the IR spectrum and vice versa. But the intramolecular charge transfer from the donor to accepter group through a single-double bond conjugated path can induce large variations of both the molecular dipole moment and the molecular polarizability, making IR and Raman activity strong at the same time. It is also observed in Methyl orange doped ZTS orange the bands in FTIR spectrum have their counterparts in Raman shows that the relative intensities in IR and Raman spectra are comparable resulting from the electron cloud movement through pi conjugated frame work from electron donor to electron acceptor groups.

Numerous natural particles that contain conjugated π electrons are portrayed hyperpolarizabilities and are dissected by method for vibrational spectroscopy [15-17]. Much of the time, even without reversal symmetry, the most grounded groups in the Raman range are feeble in the IR range and the other way around. Be that as it may, the intramolecular charge exchange from the contributor to accepter gather through a solitary twofold bond conjugated way can actuate substantial varieties of both the sub-atomic dipole minute and the sub-atomic polarizability, making IR and Raman movement solid in the meantime.

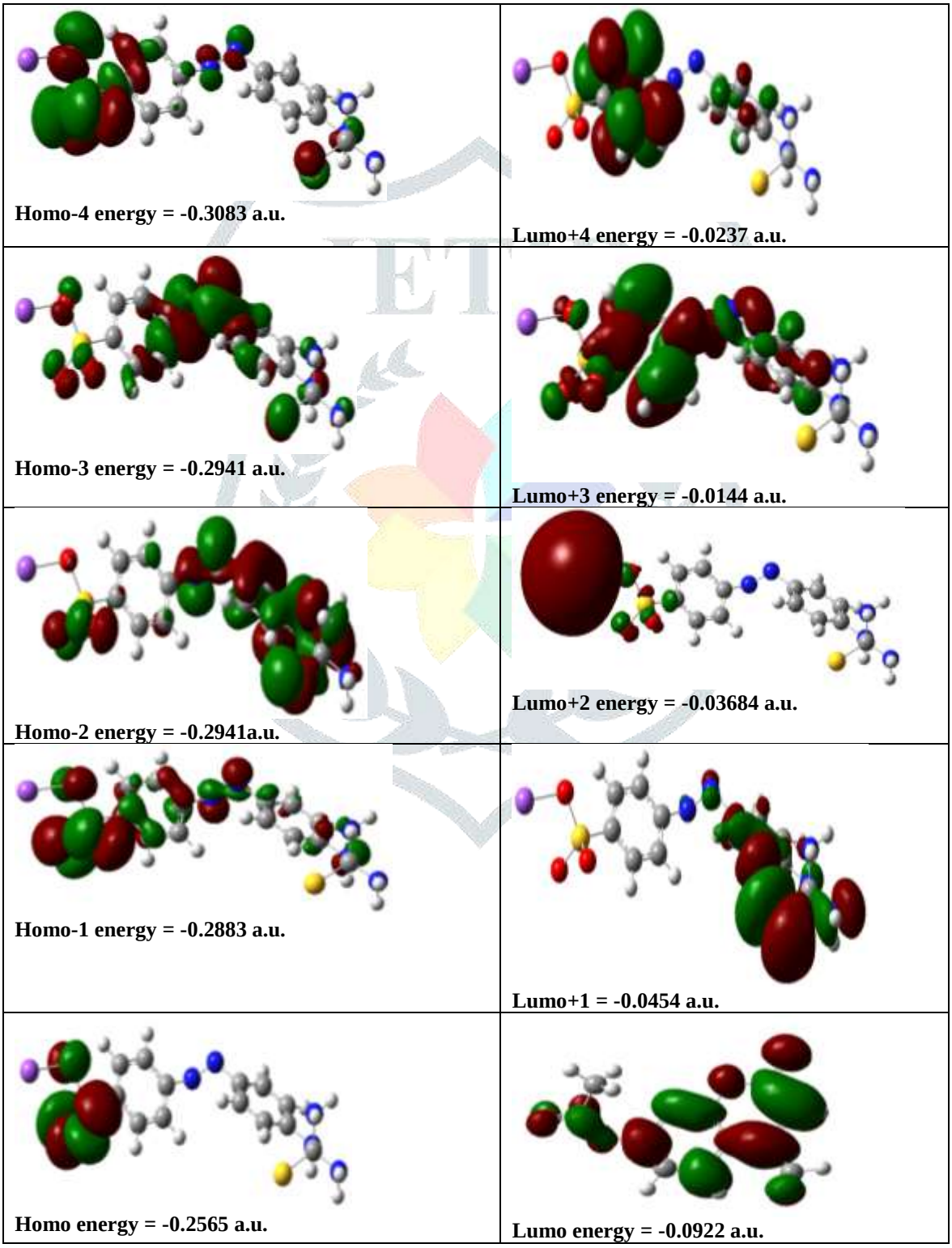

Figure 5. HOMO-LUMO plot of Methyl Red doped ZTS

It is additionally seen in Methyl Red doped ZTS orange the groups in FTIR range have their partners in Raman demonstrates that the relative powers in IR and Raman spectra are practically identical coming about because of the electron cloud development through pi

conjugated edge work from electron benefactor to electron acceptor bunches. Highest occupied molecular orbital (HOMO) and lowest unoccupied molecular orbital (LUMO) are very important parameters for quantum chemistry. We can determine the way the molecule interacts with other species; hence, they are called the frontier orbitals. HOMO, which can be thought the outermost orbital containing electrons, tends to give these electrons such as an electron donor. On the other hand; LUMO can be thought the innermost orbital containing free places to accept electrons [18]. Owing to the interaction between HOMO and LUMO orbital of a structure, transition, state transition of π^* type is observed with regard to the molecular orbital theory [19].

Therefore, while the energy of the HOMO is directly related to the ionization potential, LUMO energy is directly related to the electron affinity. Energy difference between HOMO and LUMO orbital is called as energy gap that is an important stability for structures [20]. In addition, the pictorial scheme of few MOs of Methyl orange doped ZTS is shown in Fig. 5. HOMO is localized on the central ring and has no contribution from the substitution groups such as methyl and oxygen. LUMO is quite localized on the central ring and has contribution from the substituted electronegative oxygen atom. The energy gap between HOMO and LUMO is 0.1643 a.u., which shows that charge transfer may be taking place from the ring to oxygen atom. As seen from the Fig. 5, HOMO-1 is very similar to HOMO, rotated by 90°. HOMO-3 is mainly localized on oxygen atom whereas LUMO+3 is localized on ring carbon atoms and oxygen atom.

2.7 Global and local reactivity descriptors

Based on density functional descriptors global chemical reactivity descriptors of compounds such as hardness, chemical potential, softness, electronegativity and electrophilicity index as well as local reactivity have been defined. Pauling introduced the concept of electronegativity as the power of an atom in a compound to attract electrons to it. Hardness (η), chemical potential (μ) electronegativity (χ) and softness are defined follows.

$$\eta = \tfrac{1}{2}(\partial^2 E/\partial N^2)_{V(r)} = \tfrac{1}{2}(\partial \mu/\partial N)_{V(r)}$$

$$\mu = (\partial E/\partial N)_{V(r)}$$

$$\chi = -\mu = -(\partial E/\partial N)_{V(r)}$$

where E and V(r) are electronic energy and external potential of an N-electron system respectively. Softness is a property of compound that measures the extent of chemical reactivity. It is the reciprocal of hardness.

$$S = 1/\eta$$

Using Koopman's theorem for closed-shell compounds, η, μ and χ can be defined as

$$\eta = (I - A)/2$$

$$\mu = -(I + A)/2$$

where A and I are the ionization potential and electron affinity of the compounds respectively. Electron affinity refers to the capability of a ligand to accept precisely one electron from a donor. However in many kinds of bonding viz. covalent hydrogen bonding, partial charge transfer takes places. Recently Parr *et al.* have defined a new descriptor to quantity, the global electrophilic power of the compound as electrophilicity index (ω), which defines a quantitative classification of the global electrophilic nature of a compound have proposed electrophilicity index (ω) as a measure of energy lowering due to maximal electron flow between donor and acceptor. They defined electrophilicity index (ω) as

$$\omega = \mu^2/2\,\eta$$

The usefulness of this new reactivity quantity has been recently demonstrated in understanding the toxicity of various pollutants in terms of their reactivity and site selectivity [21]. The calculated value of electrophilicity index describes the biological activity for Thiourea Methyl orange respectively. All the calculated values of HOMO-LUMO, energy gap, ionization potential, electron affinity, hardness, potential, softness and electrophilicity index are shown in Table 1 respectively.

Table 1: HOMO - LUMO energy gap and related molecular properties of Methyl Red doped ZTS

Molecular Properties	B3LYP/6-311+G(d,p)
HUMO	-0.2565
LUMO	-0.0922
Energy gap	0.1643
Ionisation Potential (I)	0.2565
Electron affinity (A)	0.0922
Global softness (s)	12.1728
Global Hardness (η□)	0.08215
Chemical potential (μ)	-0.17435
Global Electrophilicity (ω)	-0.2063

2.8 ^{13}C AND ^{1}H NMR SPECTRAL ANALYSIS

The molecular structure of ZTS is optimized by using B3LYP method with 6-311+G basis set. Then, GIAO ^{13}C calculations of ZTS are calculated and compared with experimental values [22] and that are shown in Table 1. Relative chemical shifts are then estimated by using the corresponding TMS shielding calculated in advance at the theoretical level as reference. Changes in energy needed to flip protons are called chemical shifts. The locations of chemical shifts (peaks) on a NMR spectrum are measured from a reference point that the hydrogen's in a standard reference compound – $(CH_3)_4Si$ or tetramethylsilane (TMS) – produce. The amount of energy necessary to flip protons in TMS is assigned the arbitrary value of zero δ. Chemical shifts are measured in parts per million magnetic field strength difference

(δ-scale), relative to TMS. The experimental values for ^{1}H and ^{13}C isotropic chemical shielding for TMS are 22.41 ppm and 154.54 ppm, respectively. All the calculations are performed using Gauss view molecular visualization program and GAUSSIAN 09W program package. The result shows that the range ^{13}C NMR chemical shift of the typical organic compound usually is > 100 ppm [23], the accuracy ensures reliable interpretation of spectroscopic parameters. It is true from the above literature value in our present study, that the title compound also shows the same. In practice, it is easier to fix the radio wave frequency and vary the applied magnetic field than it is to vary the radio wave frequency [24].

The magnetic field "felt" by a hydrogen atom is composed of both applied and induced fields. The induced field is a field created by the electrons in the bond to the hydrogen and the electrons in nearby π bonds. When the two fields reinforce each other, a smaller applied field is required to flip the proton. In this situation, a proton is said to be deshielded [25]. When the applied and induced fields oppose each other, a stronger field must be applied to flip the proton. In this state, the proton is shielded. Electronegative atoms such as S O, N, Na and halogens deshield hydrogens. The extent of deshielding is proportional to the electronegativity of the heteroatom and its proximity to the hydrogen. Electrons on a heterocyclic ring, double bonded atoms, and triple bonded atoms deshield attached hydrogens. These sulphur, amino and oxygen atoms show electronegative property, so the theoretical the chemical shift of C2, C3, C4, C5, C6, C15, C16,C17 and C18 seems to be 156.28, 112.63, 155.06, 126.65, 119.69, 150.80, 102.31,123.01 and 116.5 ppm for ZTS [26]. The chemical shift of C2 is greater than the other carbon values. This increase in chemical shift is due to the substitution of more electronegative oxygen and methyl atoms in the heterocyclic ring.

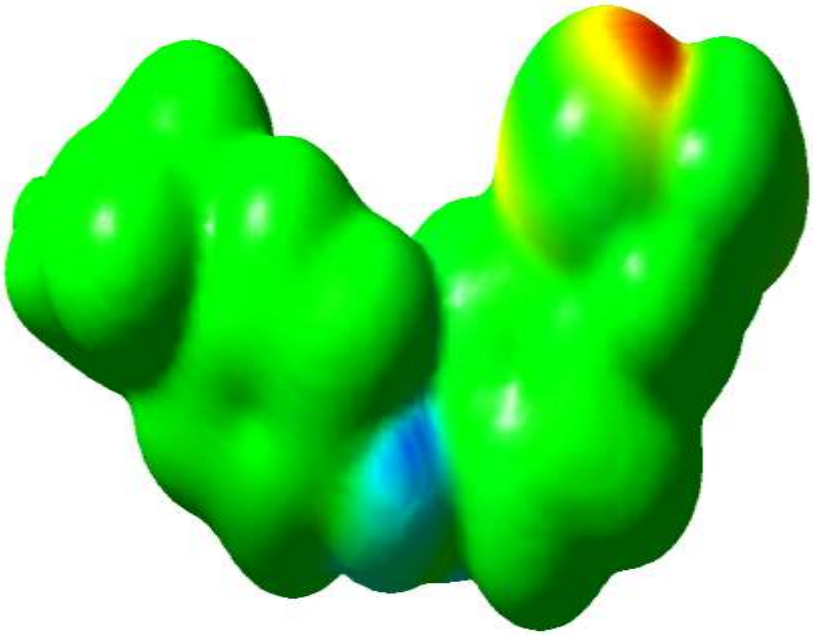

Figure 6. The molecular electrostatic potential surface of Methyl Red doped ZTS

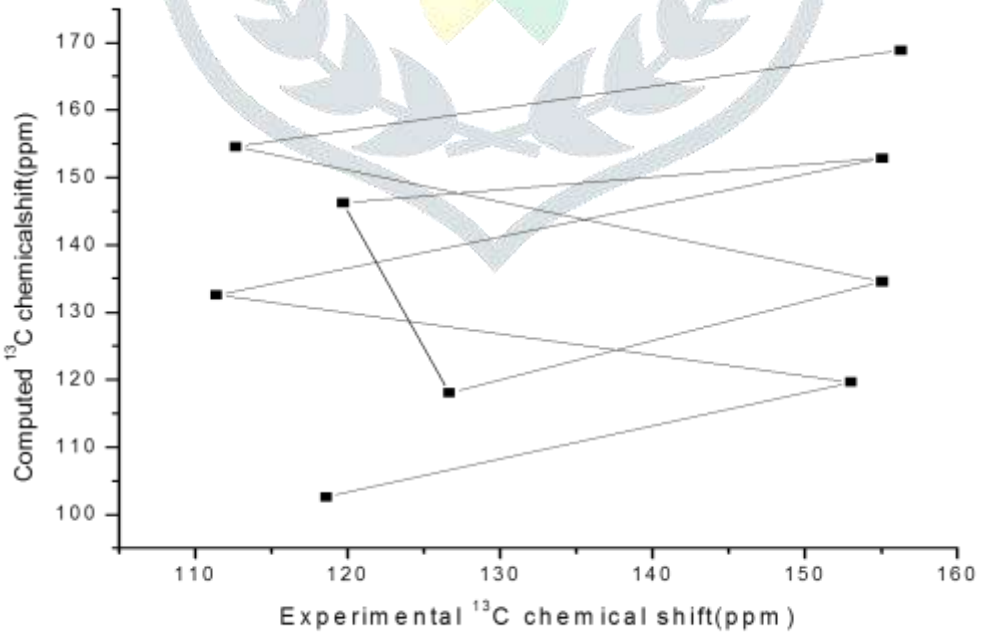

Figure 7.Comparative graph of computed and experimental of Methyl Red doped ZTS

The presence of electronegative atom attracts all electron clouds of carbon atoms towards the oxygen and methyl atoms, which leads to deshielding of carbon atom and net result in increase in chemical shift value. The NMR shielding surfaces of C4 is shown in this work (Table.2) the chemical shift (δ) for carbon atoms presented in the Methyl Red doped ZTS has been studied and theoretical ^{13}C, ^{1}H-NMR isotropic shielding of carbon and Hydrogen atom are shown. In the NMR shielding surfaces, the blue region represents shielding and

red region represents de-shielding are shown in Fig. 6. The relationship between the experimental chemical shift and computed GIAO/B3LYP/6-311+G(d,p) levels for ^{13}C are shown in Fig. 7 for doped ZTS.

Table 2. The calculated shifts of carbon and hydrogen atoms of Methyl Red doped ZTS using B3LYP/6-311+G(d,p) GIAO method

Atom position	Isotropic chemical shielding tensor (σ) (ppm)	Chemical shifts (δ) (ppm)		
		Theoretical	Expt[a]	Δ
C1	51.2597	51.259		
C2	-19.327	156.28	168.86	12.58
C3	62.2180	112.63	154.54,	41.91
C4	34.6855	155.06	134.54	-20.52
C5	57.4111	126.65	118.07	-8.58
C6	57.3342	119.69	146.23	26.54
H7	18.5263	155.06	152.86	-2.2
H8	67.9329	111.35	132.57	21.22
H9	34.7143	153.01	119.57	-33.44
H10	65.3596	118.57	102.58	-15.99
N11	-359.58	-359.58	559.58	
H12	25.5446	25.544	22.41	-3.13
N13	172.2939	13.15		
N14	30.7272	30.727	18.41	-12.31
C15	31.0491	150.80		

[a] Taken from Ref [6] and $\Delta(\delta_{exp}-\delta_{the})$; difference between respective chemical shifts.

2.9 UV-Visible studies Methyl Red doped ZTS

The UV-vis spectrum [Fig.8] of Methyl red doped ZTS was observed with the absorption bands at 278 nm in gaseous and 293 nm in alcohol. In order to understand electronic transitions in terms of energies and oscillator strengths, the TD-DFT/6-31G calculations involving configuration interaction between the singly excited electronic states were performed in the gaseous phase and in the ethanol solution (IEF-PCM model). Both the frontier molecular orbitals, highest occupied molecular orbital (HOMO) and lowest unoccupied molecular are the main orbitals taking part in chemical reaction. The electron delocalization between HOMO and LUMO is the principal factor in determining the easiness of a chemical reaction and the stereo selective path, irrespective of intra- and intermolecular process; therefore, they are the most important orbitals which help in determining the way molecule interacts with other species.

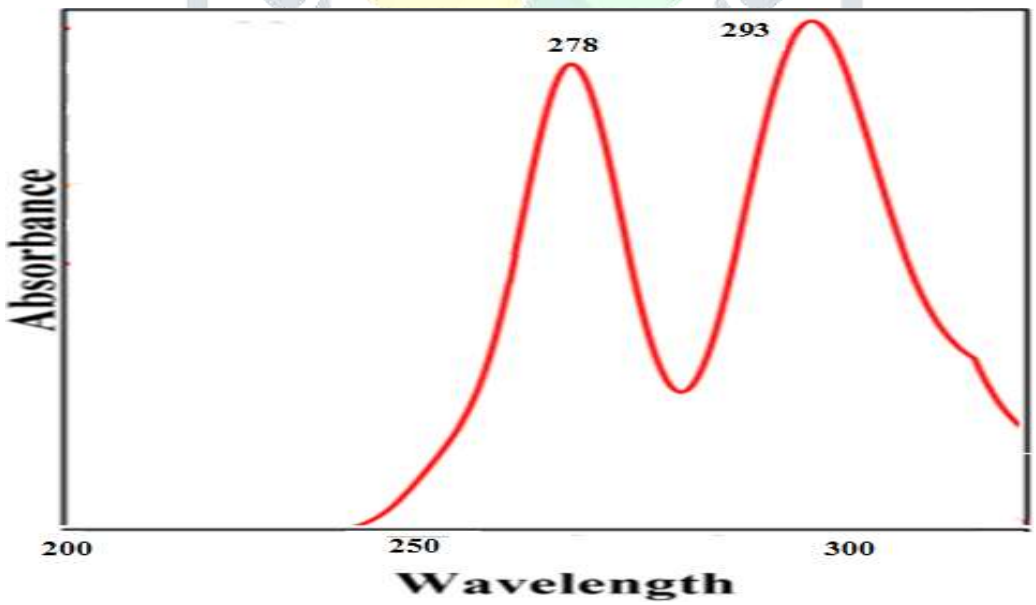

Figure 8. UV-Visible of Methyl Red doped ZTS

2.10 HOMO LUMO surfaces along with the energy gaps

The TD-DFT was employed for obtaining these FMOs. The electronic transition corresponds from HOMO (characterizes of electron giving) to the LUMO (characterizes of electron accepting) orbital. To understand the electronic transitions, positions of experimental absorption peaks, calculated wavelengths (λmax), vertical excitation energies, oscillator strengths (f), dipole moments, and excitation transition and solvent environment are carried out in Table 1. The energy gap between the HOMO and LUMO molecular orbitals characterizes the chemical reactivity and kinetic stability along with spectroscopic properties [26]. There was a difference observed in the transition orbitals on going from gaseous to solvent phase. The values for comparison are tabulated in the Table 3.

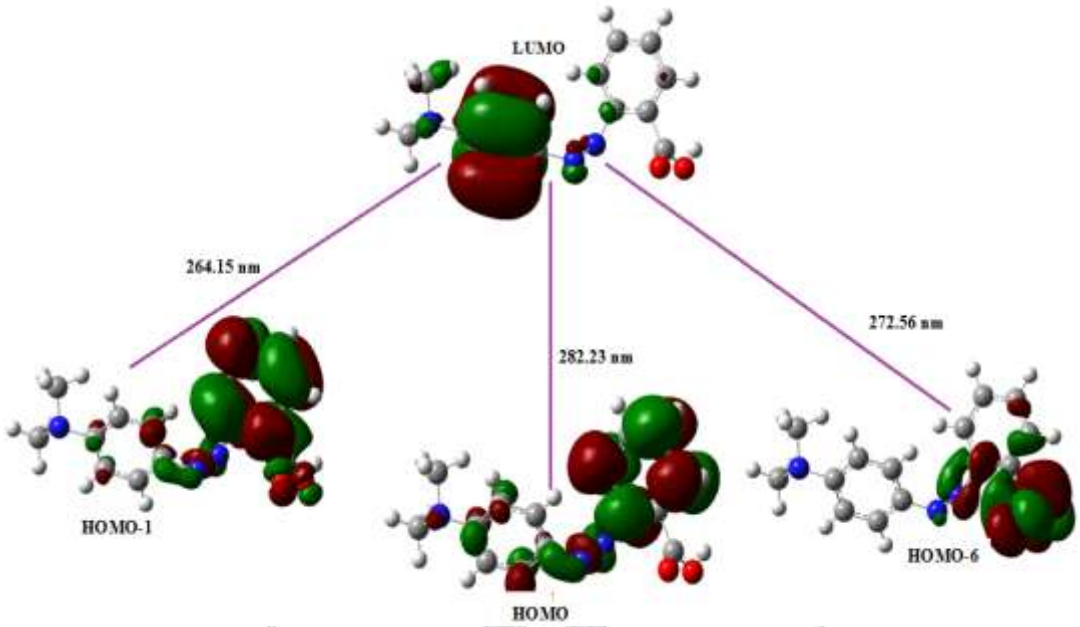

Figure 9.Plot of HOMO LUMO surfaces along with the energy gaps in ethanol.

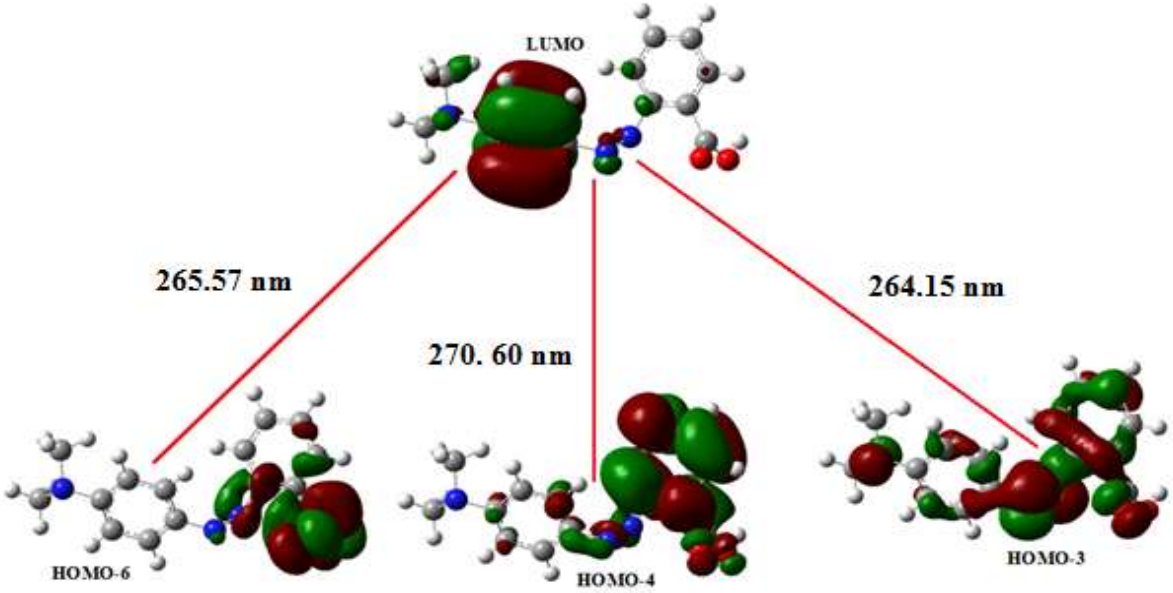

Figure 10. HOMO LUMO surfaces along with energy gaps in Isolated Gaseous phase.

Electronic absorption and Frontier Molecular orbitals (FMOs)

The transitions observed in the UV spectrum are all $\pi \rightarrow \pi^*$are shown in fig 8. From the Fig. 9 (of solvent phase) and Fig. 10 (of gaseous phase), it was clearly visible that in LUMO the charge was mainly accumulated on the C=C parts of the rings, on the nitro group both in case of isolated atom and solvent. However, in case of isolated gaseous phase in HOMO and HOMO-1 charge density along with ring is visible on the methyl group, on the O atoms and on the nitro group. In HOMO-6 it was shifted from dichloroacetamide to the hydrocarbon chain. But as far as solvent is concerned in case of HOMO-6 and HOMO-4 the charge was shifted from the ring to the hydrocarbon chain with some portions on the methyl group, whereas in HOMO-3 the whole charge was concentrated on the ring. These plots give an idea about the charge concentrations and the changes in them when dissolved in solvent. The band gap and dipole moment was also calculated for gaseous and solvent (ethanol) phase as reported in Table 3.

2.11 Molecular Electrostatic Potential (MEP).

Developing an ability to predict the structure and structure–property relations of conducting molecule in the bulk will assist the design of new structures that combine processability with favourable electronic properties. The molecular electrostatic potential (MEP) at a given point r(x,y,z) in the vicinity of a molecule can be defined as the force acting on a positive test charge (a proton) located at 'r' through the electrical charge cloud generated through the molecules, electrons and nuclei and given by the expression

$$V(r) = \sum Z_A / |R_A - r| - \int \rho(r') / |r' - r| dr'$$

where ZA is the charge on nucleus A located at RA and F (r′) is the electronic density. The first term in the expression represents the effect of the nuclei and the second represents that of electrons. MEP of a molecule has always proved to be a good guide in assessing the molecules reactivity towards positively or negatively charged reactants despite of the fact that the molecular charge distribution remains unperturbed through the external test charge (no polarization occurs). Also it is observed that there is a strong correlation of dipole moment,

electronegativity, and partial charges with electrostatic potential and by utilizing quantum mechanical calculations values could be generated for partial charges for the atoms in a molecule. Electronegativity of atoms in molecules indicates where partial charges are likely to be found - the most electronegative atoms are most negative, the others are less negative or more positive. The greater the difference in partial charges, the more polar the molecule.

The MEP provides a visual method to understand the relative polarity of a molecule through mapping total density surface on electrostatic potential energy surface. Such surfaces depict the size, shape, charge density, and site of chemical reactivity of the molecules. In the surface generated negative electrostatic potential corresponds to an attraction of the proton by the concentrated electron density in the molecules (from lone pairs, pi-bonds, etc.) (Colored in shades of red) and positive electrostatic potential corresponds to repulsion of the proton by the atomic nuclei in regions where low electron density exists and the nuclear charge is incompletely shielded (colored in shades of blue). If the surface is largely white or lightercolor shades, the molecule is mostly non-polar. Potential increases in the order red < orange < yellow < green < blue. Here we have presented the MEPs with the help of Gauss View programme .

The plot of electrostatic potential surface mapped on electron density isosurface is shown in Fig.11 for hexamer of Methyl red doped ZTS. The MEP shows that the highest negative potential visible as red blob is localized over the middle region of the two benzene rings and in the middle of the rings. Also a less negative area reflected as a yellowish blob is visible near the surrounding regions of the red portions. A very weak positive charge is localized over the above portions of the fulvene ring and could be observed as little bluish regions.

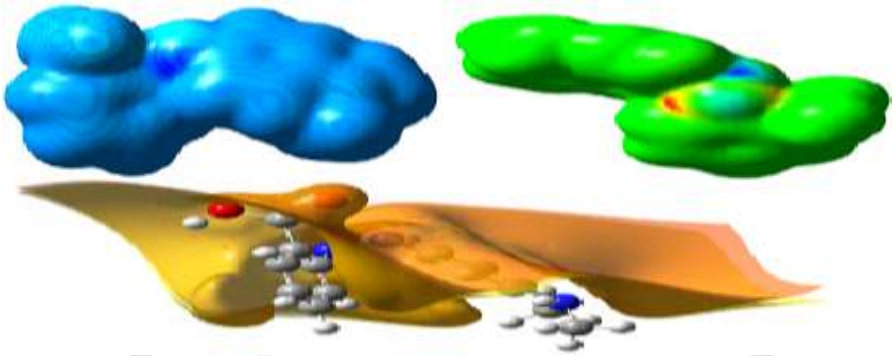

Figure 11. The molecular electrostatic potential surface of Methyl Red doped ZTS.

2.12 Thermodynamic Properties

The importance of computation of thermodynamic properties of molecules lies in thermochemistry and chemical equilibrium. The equations utilized for computing thermochemical data in Gaussian programs are derived from statistical thermodynamics with the two key ideas, the Boltzmann distribution and the partition function. The equations utilized in those programs are given in statistical mechanics texts [27-30]. The partition function is like a thermodynamic wave function, in the sense that it contains all thermodynamic information about the system, just as the quantum mechanical wave function contains all dynamic information. The total energy, zero point energy, rotational constants, dipole moment, heat capacity (Cºp,m), entropy(Sºm) and enthalpy(Hºm) of the CPP was directly obtained from the output of Gaussian programs in the optimization and vibration calculations. It was observed that the values of Cºp,m, Sºm and Hºm increases with increase in temperature from 100 K to 500 K because the molecular vibrational intensities are increasing with temperature. The correlation between temperature and these thermodynamic properties are given in Fig. 12. The correlation equations are as follows:

Cºp,m = 34.30589+0.38303T+2.69434*10-5T2 (R2=0.99957)

Sºm = 97.16984+0.68186T-0.00025T2 (R2=0.99971)

Hºm = 419.01489+0.0302T+0.0002T2 (R2=1)

These equations could be utilized in predicting the Gibbs free energy which helps when the form A is to be differentiated from the biologically active form B. Also it would help in the judgement of spontaneity of the reactions towards any reactant in which both the form A and form B would be involved. Also, the thermodynamic data would provide useful information for the study of thermodynamic energies and estimate directions of chemical reactions according to the second law of thermodynamics in thermo chemical field.

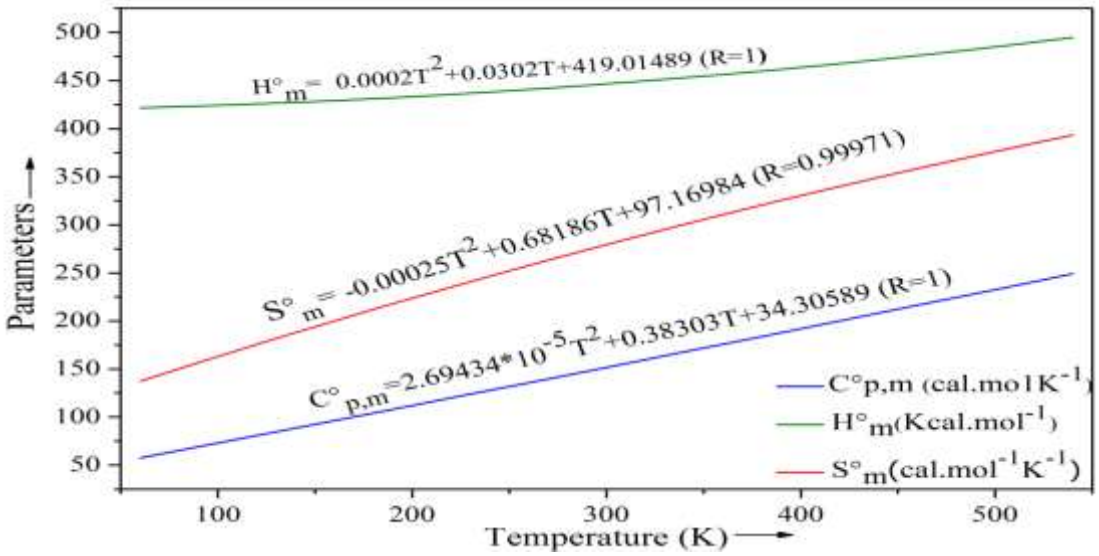

Figure 12. Correlation graphic of heat capacity (C°p,m cal.mo1K-1), enthalpy (H°m Kcal.mol-1), entropy (S°mcal.mol-1K-1) and temperature for Methyl red doped ZTS

2.11.1 Conformational studies

For the identification of all possibilities of rotational isomerism in Methyl red doped ZTS a 1-D potential energy surface (PES) scan has been performed around Φ(C6-C5-C7-C8) at B3LYP/6-31G level of theory. The PES is the mathematical or graphical relationship between the energy of a molecule (or a collection of molecules) and its geometry[31]. The scan studies were obtained by minimizing the potential energy in all geometrical parameters by varying the torsional angles at a step of 10° in the range of 0-360° rotation around the bond C5-C7. The chemical structure of Methyl red doped ZTS has two functional groups as a substituent, nitro at C11 (para position of the ring) and methyl at C5 (position 2 of the ring). These are two stereogenic centres and allow for four possible stereoisomers. But according to the literature survey, only two N are known to exist at room temperature which was very well elucidated by the double well potential energy curve (Fig. 13). It clearly shows three energy minima at -173.461°, -28.421° and 90.051° with energies -2534.86097, -2534.86006 and -2534.8571 a.u, respectively. Each energy minimum can be associated to Methyl red doped ZTS; the former well is deeper than the other two and thus it represents the most stable conformation to be called conformer. If we consider the two methyl group as fixed, then the ring is in trans conformation to the hydrocarbon chain in conformer and in cis conformation in conformer[32].

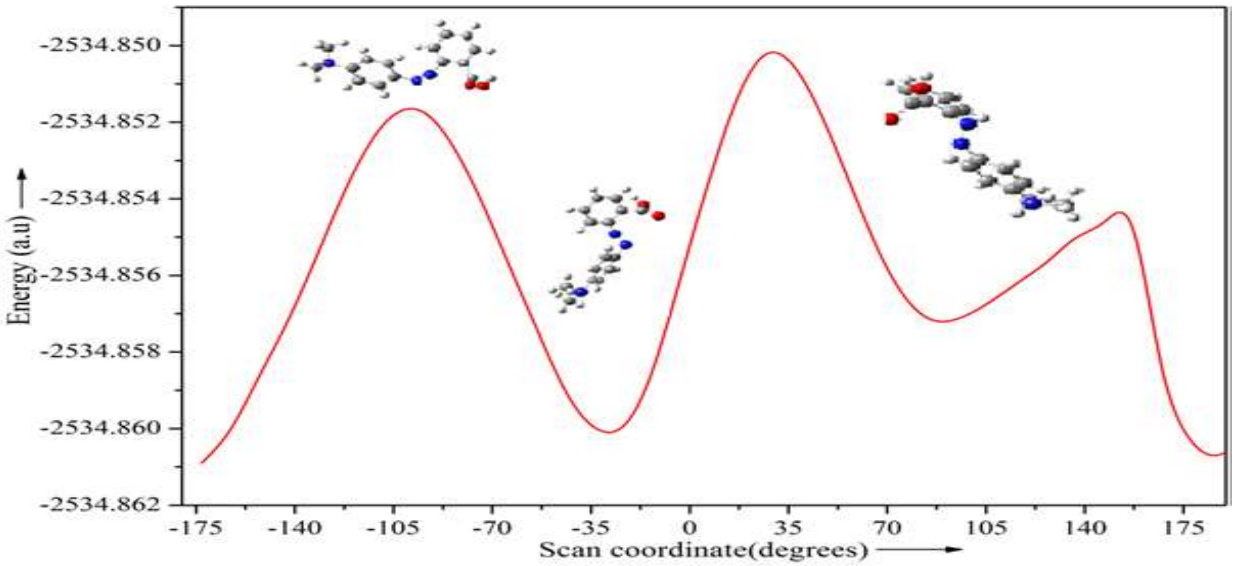

Figure 13 . Potential energy curve of Methyl red doped ZTS as a function of the angle ϕ (C6-C5-C7-C8) clearly showing the conformer.

Table 3. Electronic transitions, absorption wavelength λmax (nm), excitation energy (eV), oscillator strengths (f), frontier orbital energies (eV) and dipole moment (Debye) of ZTS + Methyl red .

Excited States	Excitation Transition						λmax (nm)		E(ev)	Oscillatory strength (f)				Transition type/ assignments
	Gas phase		Ethanol				Experimental			Calculated	Gas phase	Ethanol		
							Water		Ethanol	Gas phase	Ethanol			
1	150 →151	H→L	146→151	H-4→L						282.95	270.60	4.382	4.582	0.033	0.007	π → π*
2	147→151	H-3→L	147→151	H-3→L	278	293				273.23	265.57	4.538	4.669	0.060	0.001	π → π*
3	149→151	H-1→L	144→151	H-6→L						264.15	259.21	4.694	4.783	0.056	0.0	π → π*

												56	
		EHOMO (eV)	ELUMO (eV)	ΔE (eV)	μ (D)								
	Gas	-7.637855	-2.7243	-4.91349	5.6374								
	Ethanol	-7.317037	-2.7461	-4.57090	6.9082								

2.13 NLO STUDIES

The dye doped ZTS crystals are used for the generation of second harmonics by Nd-based near-infrared solid-state lasers. The fundamental of an Nd:YAG laser (1064 nm) can be converted to 532 nm of second harmonic or its 355 nm of third harmonic or its 266 nm of fourth harmonic by using GLS crystals[33]. The performance of these frequency conversion devices can be seriously degraded, if there are any defect-associated, the absorption bands in the crystal which overlap the fundamental pump wavelength or one of the output wave lengths. Thus, it is important to identify and characterize all potentially harmful absorption bands in non-linear optical crystals. In order to confirm the suitability of the doped ZTS crystal, the non-linear application, harmonic generation was tested by using the Nd-YAG laser [34-36]. A small crystal was placed on the sample holder and the YAG laser beam was made to pass through the crystal and the output conversion of input as green light SHG was analyzed. The crystals are used for the generation of harmonics of Nd-based near-infrared solid-state lasers .The fundamental of an Nd:YAG laser (1064 nm) can be converted to 532 nm of second harmonic or its 355 nm of third harmonic or its 266 nm of fourth harmonic by using KDP crystals.

An important related property of NLO crystals is the threshold for catastrophic laser induced damage. Laser induced damage in optical materials is a phenomenon involving interaction of high power laser radiation with matter and various physical, chemical, mechanical, optical and other aspects of materials come into role play. It is evident that the harmonic conversion efficiency is proportional to the power density of the fundamental beam. Hence, a convenient way to increase the efficiency is to focus the beam into the crystal. But, this often leads to breakdown of the materials, catastrophically damaging the crystal. It is then useful to prescribe the maximum permissible power for a particular crystal, defined as damage threshold [37].

It is believed that the formation of an ionized region of dense plasma is the first and the most important step in a damage event. In recent times, there have been several effects to model the laser damage processes by taking the pulse shape and duration in to account. Laser damage in general manifests itself as a localized microscopic entity. Microscopic examination of the damage sites created in different materials often suggests the mechanism responsible for such a process [38].

The performance of these frequency conversion devices can be seriously degraded if there are defect-associated absorption bands in the crystal which overlap the fundamental pump wavelength or one of the output wave lengths [39]. Thus, it is important to identify and characterize all potentially harmful absorption bands in non-linear optical crystals [40].

In order to confirm the suitability of the doped ZTS crystal for non-linear applications, second harmonic generation was tested using the Nd-YAG laser. A small crystal was placed on the sample holder and the YAG laser beam was made to pass through the crystal and the output (green light SHG) was analyzed. The SHG efficiency of Methyl Red doped ZTS was maxima among the investigated pure and doped ZTS crystals. The SHG efficiency of pure ZTS and Methyl Red dye doped ZTS were tabulated in Table 4.

Table 4. Comparison of SHG of pure and Methyl Red doped ZTS Crystals

S.No.	Compound	SHG efficiency
1.	ZTS Crystals	1.56
2.	Methyl Red doped ZTS crystals	1.93

The efficiency of doped ZTS crystals were compared with pure ZTS and also show that dye doped ZTS crystal has higher efficiency. A sample of ZTS, also powdered was used for the same experiment as a reference material in the SHG measurement. It was found that the frequency doubling efficiency of the doped ZTS is better than KDP.

3 CONCLUSION

The dye doped ZTS crystals are used for the generation of second harmonics of Nd-based near-infrared solid-state lasers. The fundamental of an Nd:YAG laser (1064 nm) can be converted to 532 nm of second harmonic or its 355 nm of third harmonic or its 266 nm of fourth harmonic by using ZTS crystals. The performance of these frequency conversion devices can be seriously degraded if there are defect-associated absorption bands in the crystal which overlap the fundamental pump wavelength or one of the output wave lengths. Thus, it is important to identify and characterize all potentially harmful absorption bands in non-linear optical crystals. In order to confirm the suitability of the doped ZTS crystal, the non-linear application, harmonic generation was tested using the Nd-YAG laser. The HOMO–LUMO energy gap calculated at the B3LYP/6-311++G(d,p) level reveals the chemical activity and kinetic stability of the molecule. The large negative ESP is observed at oxygen atom in the compounds and this starts to spreads near hydrogen atom under the increase of field. The NBO analysis indicates the intramolecular charge transfer between the bonding and antibonding orbitals. The NBO analysis indicates the intramolecular charge transfer between the bonding and antibonding orbitals. This implies that the electrophillic attack is also taking place at hydrogen atom as field increases. The corresponding maps from the theoretical analysis explain similar features. Single crystals grown by the various methods need to be characterized to assess the suitability of the crystal for various applications including NLO

applications. A sample of ZTS, also powdered was used for the same experiment as a reference material in the SHG measurement. It was found that the frequency doubling efficiency of the doped ZTS was better than KDP.

Acknowledgement

We gratefully acknowledge financial supports from the Department of Science & Technology-Science and Engineering Research Board [DST-SERB-FAST TRACK, PS-20/2009(SR)], New Delhi, India.

References

[1] J.Ramajothi, S. Dhanuskodi and K. Nagarajan, Crystal Research and Technology,39(2004) 414.
[2] T. C. Sabari Girisun and S. Dhanuskodi, Crystal Research and Technology, 44(2009)1297.
[3] S. Selvasekarapandian, K. Vivekanandan, P. Kolandaivel and T. K. Gundurao, Crystal Research and Technology, 32(1997) 299.
[4] P.M. Ushasree, R. Jayavel, C. Subramanian, P. Ramasamy, Journal of Crystal Growth,197(1999)216.
[5] H. O. Marcy, L. F. Warren, M. S. Webb, C. A. Ebbers, S. P. Velsko, G. C. Kennedy, and G. C. Catella, OSA Publishing - Applied Optics , Volume 31, Issue 24, Page 5051.
[6] V. Venkataramanan, G. Dhanaraj, V.K. Wadhawan, J.N. Sherwood, H.L. Bhat, Journal of Crystal Growth, 154(1995)92.
[7] S. S. Gupte and C. F. Desai, Crystal Research and Technology, 34(1999)1329.
[8] P.M Ushasree, R Muralidharan, R Jayavel, P Ramasamy ,Journal of Crystal Growth, 210(2000)741.
[9] H. Nakatani and W. R. Bosenberg, Appl. Phys. Lett. 53(1988)2587.
[10] S. S. Gupte and C. F. Desai, Cryst. Res. Technol. 34(1999)1329.
[11] V. Venkataramanan and G. Dhanaraj, Ferroelectrics 155(1994)13.
[12] P. R. Newman, L. F. Warren, P. Cunningham, T. Y. Chang, D. E. Cooper,
[13] G. L. Burdge, P. Polak-Dingels, and C. K. Lowe-Ma, Mater. Res. Sot.Symp. Proc. 173(1990)557.
[14] H. 0. Marcy, L. F. Warren, M. S. Webb, C. A. Ebbers, S. P. Velsko, G. C.Kennedy, and G. C. Catella, Appl. Opt. 31 (1992)505.
[15] U. Ramabadran, David E. Zelmon, and G. C. Kennedy, Appl. Phys. Lett.60(1992)2589.
[16] P. Yankov, D. Schumov, A. Nenov, and A. Monev, Opt. Lett. 18(1993)1771.
[17] A. Yokotani, T. Sasaki, K. Yoshida, and S. Nakai, Appl. Phys. Lett. 55 (1989)2692.
[18] F. Mauro, J. Opt. A: Pure Appl. Opt. 1(1999)662.
[19] S. S. Gupte, A. Marcano O., R. D. Pradhan, and N. Melikechi, J. Appl.Phys. 89(2001)4939.
[20] V. Venkataramanan, G. Dhanaraj, V. K. Wadhawan, J. N. Sherwood, and H. L. Bhat, J. Cryst. Growth 154(1995)92.
[21] A. V. Alex and J. Philip, J. Appl. Phys. 90(2001)720.
[22] K. Vasantha and S. Dhanuskodi, Spectrochemica Acta Part A 58 (2002)311.
[23] S. Selvasekarapandian, K. Vivekanandian, P. Kolandaivel, and T. K. Gundurao, Cryst. Res. Technol. 32 (1997) 299.
[24] R. M. Silverstein, G. Clayton Basseler, and T. C. Morrill, Spectrometric Identification of Organic Compounds, VEdn.John Wiley & Sons, Inc. New York 1998.
[25] H. O. Marcy, M. J. Rosker, L. F. Warren, P. H. Cunningham, C. A. Thomas, L. A. Deloach, S. P. Velsko, C. A. Ebbers, J. H. Liao, and M. G. Kanatzidis, Opt. Lett. 20(1995) 252.
[26] R. C. Heckman, J. Appl. Phys. **44**, 1455 -1973.
[27] N. J. Long, Angew. Chem. 34(1995) 21.
[28] K.Sambathkumar, A.Claude and K.Settu Elixir Vib. Spec.91(2016) 38368.
[29] M.Rajasekaran, P.Kumaresan and K.Sambathkumar Elixir Comp. Chem. 92 (2016) 39051 .
[30] E. Elamurugu Porchelvi, S. Muthu, J. Spectrochim., Acta., 134 (2015) 4530.
[31] K.Sambathkumar, S.Jeyavijayan M .Arivazhagan; Spectrochim. Acta A 147 (2015)51.
[32] R. Mohan Kumar, D. Rajan Babu, D. Jayaraman, R. Jayavel, and K. Kitamura, J. Cryst. Growth 275.
[33] Tiffany N.Thomas,Terry A Land, Michael Johnson, William H Casey, Journal of Colloid and Interface Science 280, 18 (2004).
[34] G. Bhagavannarayana, S.K. Kushwaha, S. Parthiban, S. Meenakshisundaram, J. Cryst.Growth 311, 960 (2009).
[35] M. Lawrence, Thomas Joseph Prakash, J. Spectrochimica Acta Part A 91, 30 (2012).
[36] K.Sambathkumar, Elixir Vib. Spec. 91 (2016) 38381.
[37] K.Sambathkumar, S.Jeyavijayan, M. Arivazhagan; Spectrochim. Acta A 147 (2015)51-66.
[38] R. T. Bailey, F. R. Cruickshank, P. Kerkoc, S. Lochran, D. Pugh, J. N. Sherwood, A. J. Blake, and S. Parsons, J. Appl. Phys. **78**, 3102-1995.
[39] Kuppusamy Sambathkumar, Spectrochim. Acta A 147 (2015) 51-66.
[40] H. Groot, in Thermal Conductivity 20, edited by D. P. H. Hasselman and J. R. Thomas, Jr. ~Plenum, New York, 1989!, pp. 357–388.
[41] K. Sambathkumar, S. Nithiyanantham, J Mater Sci: Mater Electron 2017,28, 6529–6543.
[42] T. Wojtatowicz and K. Rozniakowski, in Thermal Conductivity 20, edited by D. P. H. Hasselman and J. R. Thomas, Jr. Plenum, New York, 1989, pp. 367–375.